

Classical Rules for Qubit Spin-Rotation Error Suppression.

Qile Su

¹*Department of Physics and Astronomy, University of California, Los Angeles, CA 90095, USA*

A frequently encountered source of systematic error in quantum computations is imperfection in the control pulses that function as logical quantum gates for qubits. It was demonstrated that *composite* pulses can mitigate certain systematic errors and an appealing geometric interpretation was developed for the design of error-suppressing composite pulses. In this paper it is shown that this geometric method can be obtained from a simple perturbation analysis of classical Larmor precession. The derivation is straightforward and requires only a minimal understanding of quantum mechanics, making it accessible to undergraduates who had an intermediate quantum mechanics course.

I. INTRODUCTION

A typical quantum logical gate is the single-qubit NOT gate, realized by a π -pulse. The action of a π -pulse amounts to the rotation of the Bloch vector of the qubit by π through the application of an AC control pulse. Actual gates applied to a qubit can be imperfect because of lack of control of the pulse in terms of amplitude, duration, frequency and phase [1]. In addition, coupling between a qubit and its environment generates inelastic interactions, which can introduce random errors through phase decoherence [2–4]. This paper is limited to two frequently encountered systematic errors namely imperfect control of the amplitude of the pulse, or *amplitude error*, and imperfect control of the frequency of the pulse, or *detuning error*¹.

Following work by the NMR community, it has been demonstrated experimentally that amplitude and detuning errors can be reduced by replacing a single π -pulse by *composite* pulses [5, 6] and it was shown mathematically [1] that an amplitude error of order ϵ incurred during the rotation of a Bloch vector by π could – at least in principle – be reduced to an error of the order of ϵ^n , with n an integer, by breaking the π -pulse up into a sequence of $2n$ rotations of the Bloch vector over π or 2π . General constraints were derived on the control pulse that, if obeyed, should reduce the amplitude error and detuning error, and a geometrical interpretation of these constraints was developed [7, 8]. An experimental search for sequences that suppress both the amplitude and the detuning error [6] led to the so-called *Knill sequence*, a sequence of five π -pulses that is further discussed below. Using the geometrical interpretation, it has been shown that this Knill sequence is a member of a broader, one-parameter family of sequences that eliminate the leading order amplitude and detuning errors simultaneously [7].

As might be expected, the mathematical analyses of the error-suppressing procedures were based on the general principles of quantum mechanics. In this paper we develop a *classical* framework for the construction of composite sequences composed of π -pulses. The starting point is the Ehrenfest

Theorem that translates the quantum dynamics of spin 1/2 operators to the classical dynamics of the spin operator expectation value. Through a perturbation analysis of the classical precession of the Bloch vector, constraints are derived on a sequence that, when obeyed, suppress the lowest-order amplitude and detuning errors. It is shown that these constraints are fully equivalent to the ones obtained from the complete quantum mechanical analysis. Using only simple vector algebra, the method can be applied to design composite pulses that suppress either or both amplitude and detuning errors.

Section II develops a second-order perturbation expansion for the equation of motion of the Bloch vector during a given sequence due to perturbations generated by amplitude and detuning errors. Expressions are derived for the two global constraints that must be obeyed if first and second-order amplitude and detuning errors are to be eliminated, respectively. In Section III the first-order constraint is illustrated for a variety of sequences, and the equivalence between the quantum and classical methods is demonstrated for the case of the first-order constraint. In Section IV, the second-order constraint is illustrated for a number of sequences and it is shown that the classical and quantum constraints are also equivalent to second-order. We conclude in Section V.

II. DYNAMICS OF THE BLOCH VECTOR AND PERTURBATION THEORY.

The specific realization of a qubit considered in this paper is a spin-1/2 two-level system in a DC magnetic field along the z direction. The level splitting is $\hbar\omega_0$ with ω_0 the Larmor frequency. Let the spinor $|\psi\rangle = (\alpha, \beta)$ denote the general spin state $\alpha|\uparrow\rangle + \beta|\downarrow\rangle$. A π -pulse is performed by the application of an AC magnetic field rotating in the xy -plane with frequency ω and phase ϕ [9]. In terms of the Pauli matrices the spin Hamiltonian can be expressed as

$$H = \hbar/2[\omega_0\hat{\sigma}_z + \Omega_0 \cos(\omega t + \phi)\hat{\sigma}_x + \Omega_0 \sin(\omega t + \phi)\hat{\sigma}_y], \quad (1)$$

where Ω_0 is the magnitude of the AC magnetic field in frequency units. A perfect π -pulse has frequency $\omega = \omega_0$ and duration π/Ω_0 (a π -pulse). If the drive frequency ω differs from ω_0 , then a detuning error results while an amplitude error results if the pulse duration differs from π/Ω_0 , or if the actual AC field strength differs from Ω_0 , or both. After performing the standard rotating wave approximation (see appendix A for

¹ Depending on the context, amplitude errors may also be known as flip-angle errors or pulse-length errors, while detuning errors are also known as off-resonance errors or frequency offsets.

details) the effective Hamiltonian reduces to that of a spin-1/2 particle in a time-independent magnetic field:

$$H' = \hbar/2[\Delta\hat{\sigma}_z + \Omega_0 \cos \phi \hat{\sigma}_x + \Omega_0 \sin \phi \hat{\sigma}_y]. \quad (2)$$

This field $\Omega = (\Delta, \Omega_0 \cos \phi, \Omega_0 \sin \phi)$ (in frequency units) has a z component $\Delta = \omega_0 - \omega$ that is the detuning error while the projection of the field in the xy -plane makes an angle ϕ with the x -axis². For convenience, this frame after the rotating wave approximation will be referred to as the ‘‘lab frame’’ though it actually rotates with respect to the real laboratory frame. In the following we will use units with dimensionless time (i.e., $\Omega_0 t$) and dimensionless transverse field strength.

Using the Ehrenfest Theorem, it is shown in appendix A that in the lab frame the expectation value $\mathbf{r}(t)$ of the spin operator (the Bloch vector) obeys the classical equation of motion for the Larmor precession of a magnetic moment in a magnetic field:

$$\frac{d\mathbf{r}(t)}{dt} = \Omega(t) \times \mathbf{r}(t). \quad (3)$$

In the following, we will separate the error-free (or ‘‘nominal’’) part of the pulse $\Omega(t)$ from the amplitude and detuning errors $\Omega_1(t)$, so

$$\frac{d\mathbf{r}(t)}{dt} = (\Omega(t) + \Omega_1(t)) \times \mathbf{r}(t). \quad (4)$$

Amplitude errors are represented as $\Omega_1(t) = \epsilon\Omega(t)$, which changes the rotation rate induced by the control pulse by a factor of $(1 + \epsilon)$ while detuning errors are represented as $\Omega_1(t) = \Delta\hat{\mathbf{z}}$, always pointing along the z direction. The quantities ϵ and Δ will be assumed to be constant over the duration of the sequence and to be small compared to one.

Figure 1 shows the motion of the Bloch vector for the case of a $\pi/2$ pulse with transverse field along the y direction. The initial orientation of the spin is again along the z direction. The black trajectory is the ‘‘nominal’’ (i.e., error-free) case while the red trajectory shows the deviation induced by a non-zero detuning error. The time-evolution of the error, a problem that becomes only more serious as the complexity of the sequence increases. This can be circumvented by introducing the toggling frame, an intermediate representation that subtracts out the nominal motion caused by $\Omega(t)$. Denoting the time-dependent transformation matrix between the lab frame and the toggling frame as $\hat{\mathbf{R}}(t)$. Then coordinates in the lab frame (un-primed) and those in the toggling frame satisfies $\mathbf{v}(t) = \hat{\mathbf{R}}(t)\mathbf{v}'(t)$. At $t = 0$, $\hat{\mathbf{R}}(t)$ satisfies $\hat{\mathbf{R}}(0) = \hat{\mathbf{I}}$, so $\mathbf{r}'(0) = \mathbf{r}(0)$. In appendix B it is shown that the equation of motion of the Bloch vector in the toggling frame is

$$\frac{d\mathbf{r}'(t)}{dt} = \Omega_1'(t) \times \mathbf{r}'(t). \quad (5)$$

² Time-dependent terms with frequency $2\omega_0$ are discarded in this transformation.

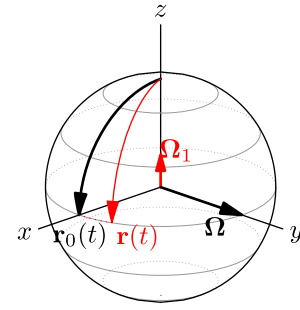


FIG. 1. Motion of the Bloch vector in the lab frame for a $\pi/2$ pulse about the y -axis in the presence of a detuning error [see Eq.(4)]. Black trajectory: nominal motion $\mathbf{r}_0(t)$ for zero detuning error. Red trajectory: motion in the presence of a detuning error Ω_1 . The gray circles on the Bloch sphere are contours of constant angle from the spin up direction.

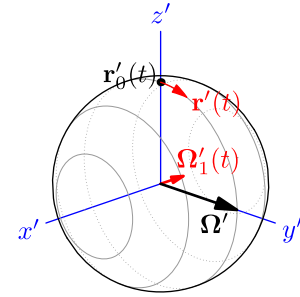


FIG. 2. Motion of the Bloch vector (Eq.(5)) in the toggling frame (blue, primed axes) for the same $\pi/2$ rotation about the lab frame y -axis as in figure 1. Red vector: the detuning error vector $\Omega_1'(t) = \Delta \hat{\mathbf{R}}^{-1}(t)\hat{\mathbf{z}}$, which is time-varying. Red trajectory: motion of the Bloch vector $\mathbf{r}'(t)$ in the toggling frame. The gray circles show the orientation of the Bloch sphere in the toggling frame for the final state, corresponding to the gray circles in the previous figure.

Amplitude error $\Omega_1(t)$ remains piecewise constant when transformed into $\Omega_1'(t)$ in the toggling frame. Conversely, while the detuning error is time-independent in the lab frame, it becomes time-dependent in the toggling frame. Figure 2 compares the motion of the Bloch vector in the lab frame with the motion in the toggling frame for the case of detuning error.

The next step is to construct a perturbation expansion by multiplying the error vector $\Omega_1'(t)$ by the small parameter w , which later can be set to one, and expanding the Bloch vector in powers of w :

$$\mathbf{r}'(t) = \mathbf{r}'_0(t) + w\mathbf{r}'_1(t) + w^2\mathbf{r}'_2(t) + \dots \quad (6)$$

Inserting in the equation of motion in the toggling frame gives

$$\frac{d\mathbf{r}'(t)}{dt} = w \Omega_1'(t) \times \mathbf{r}'(t). \quad (7)$$

Collecting terms to the same order in w gives the set of equa-

tions

$$\frac{d\mathbf{r}'_0(t)}{dt} = 0 \quad (8)$$

$$\frac{d\mathbf{r}'_1(t)}{dt} = \boldsymbol{\Omega}'_1(t) \times \mathbf{r}'_0(t) \quad (9)$$

$$\frac{d\mathbf{r}'_2(t)}{dt} = \boldsymbol{\Omega}'_1(t) \times \mathbf{r}'_1(t) \quad (10)$$

...

Integrating the zero-order, first-order and second-order equations gives

$$\mathbf{r}'_0(t) = \mathbf{r}_0(0) \quad (11)$$

$$\mathbf{r}'_1(t) = \int_0^t \boldsymbol{\Omega}'_1(s) \times \mathbf{r}_0(0) ds \quad (12)$$

$$\mathbf{r}'_2(t) = \int_0^t \boldsymbol{\Omega}'_1(s) \times \mathbf{r}'_1(s) ds \quad (13)$$

...

with $\mathbf{r}_0(0)$ the initial orientation of the Bloch vector. A sequence thus suppresses error to the second order error if it obeys the two constraints for the error of interest,

$$\int_0^{t_f} \boldsymbol{\Omega}'_1(s) \times \mathbf{r}_0(0) ds = 0, \quad (14)$$

$$\int_0^{t_f} \boldsymbol{\Omega}'_1(s) \times \mathbf{r}'_1(s) ds = 0, \quad (15)$$

with t_f the duration of the sequence. Note that evaluating the integral in the second-order constraint requires information about the first-order perturbation $\mathbf{r}'_1(t)$ over the entire sequence. Constructing sequences that obey these two constraints is the subject of the next two sections.

III. THE FIRST-ORDER CONSTRAINT.

In this section we focus on the first-order constraint, illustrating how it works for a number of different sequences and then obtain general geometrical rules for first-order error suppression. These rules are then compared with the ones that were obtained earlier in literature directly from quantum mechanics.

First define the “error integral” $\mathbf{p}(t)$ to be

$$\mathbf{p}(t) = \int_0^t \boldsymbol{\Omega}'_1(s) ds, \quad (16)$$

where the upper bound of the integration is allowed to vary. The function $\mathbf{p}(t)$ can be viewed as describing the trajectory of a phantom particle moving in the toggling frame with velocity $\boldsymbol{\Omega}'_1(t)$, starting from the origin at $t = 0$. Substitute the definition of $\mathbf{p}(t)$ into the first-order constraint Eq.(14):

$$\mathbf{r}'_1|_{t=t_f} = \mathbf{p}|_{t=t_f} \times \mathbf{r}_0(0) = 0. \quad (17)$$

In addition, define separate step “error integral vectors” \mathbf{p}_i for the individual steps of the sequence:

$$\mathbf{p}_i = \int_{t_i}^{t_{i+1}} \boldsymbol{\Omega}'_1(s) ds, \quad (18)$$

with t_i and t_{i+1} the initial and final times of pulse i . Using this definition in Eq.(17) finally yields the condition for first-order error suppression

$$\mathbf{r}'_1|_{t=t_f} = \left(\sum_i^N \mathbf{p}_i \right) \times \mathbf{r}_0(0) = 0. \quad (19)$$

If the trajectory $\mathbf{p}(t)$ is closed, i.e., if the end point $\mathbf{p}|_{t=t_f}$ of the trajectory is the starting point (the origin), then the first-order constraint is obeyed *for all initial conditions* $\mathbf{r}_0(0)$. Such sequences are “fully-compensating” [1]. The suppression of error regardless of initial condition is also known as “universality” [9]. Suppose the sequence is composed of N steps. The vectors \mathbf{p}_i define an N -step walk in space when placed head-to-tail. The sequence is fully-compensating if this N -step walk is closed.

A. Spin-echo Sequence

Our first example is the three-step *spin-echo* sequence [10]. The short-hand notation R_ϕ^θ will be used to denote a single pulse, with ϕ the direction of the pulse in the xy -plane and θ the duration of the pulse. An error-free π -pulse around x is denoted as R_0^π . The spin echo sequence is denoted as $R_0^{\pi/2} \rightarrow R_{\pi/2}^\pi \rightarrow R_0^{\pi/2}$. It has the following time-dependent pulse direction $\boldsymbol{\Omega}(t)$:

$$\boldsymbol{\Omega}(t) = \begin{cases} \hat{x} & t \in (0, \frac{\pi}{2}) \\ \hat{y} & t \in (\frac{\pi}{2}, \frac{3\pi}{2}) \\ \hat{x} & t \in (\frac{3\pi}{2}, 2\pi) \end{cases}. \quad (20)$$

In the presence of amplitude or detuning error, the first step is calculating the error $\boldsymbol{\Omega}'_1(t)$ in the toggling frame. This is easy for the amplitude error case because the error is always parallel to the pulse direction $\boldsymbol{\Omega}'(t)$, which in turn is step-wise constant in the toggling frame. The three vectors corresponding to the values taken by the pulse direction $\boldsymbol{\Omega}'(t)$ are shown in figure 3(a). The error integral vectors \mathbf{p}_i are directed along the three vectorial values taken by the error $\boldsymbol{\Omega}'_1(t)$. The resulting three-step walk is shown in figure 3(b). Note that the vector for step II has twice the length of that of steps I and II because it is a full π -pulse rather than a $\pi/2$ pulse. The three-step walk is not closed so the first-order constraint is not obeyed.

For the case of the detuning error, $\boldsymbol{\Omega}_1$ is constant in the lab frame, pointing in z with magnitude Δ , but in the toggling frame the direction of $\boldsymbol{\Omega}'_1(t) = \hat{\mathbf{R}}^{-1}\boldsymbol{\Omega}_1$ rotates at a constant rate. This apparent motion is the result of the rotation of the toggling frame, and is shown in figure 4. Note that the figure 4(a) resembles the rotation of the Bloch vector on the Bloch

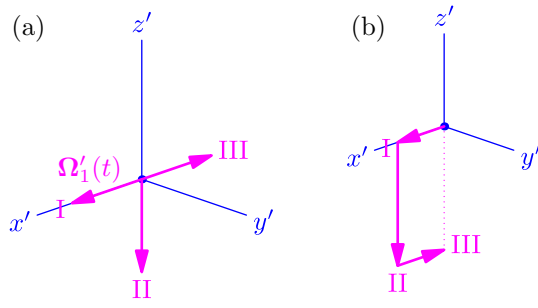


FIG. 3. (a): the amplitude error $\Omega'_1(t)$ (pink) for the spin-echo sequence $R_0^{\pi/2} \rightarrow R_{\pi/2}^{\pi} \rightarrow R_0^{\pi/2}$ in the toggling frame. The three steps of the sequence are labelled I, II, and III. All three vectors should have length ϵ . (b): the three-step walk consists of the error integral vectors \mathbf{p}_i for the spin-echo sequence with amplitude error.

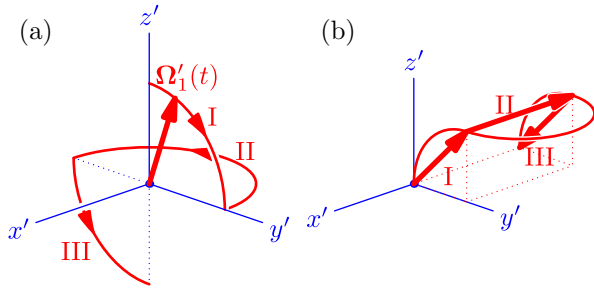


FIG. 4. (a): the detuning error $\Omega'_1(t)$ for the spin-echo sequence $R_0^{\pi/2} \rightarrow R_{\pi/2}^{\pi} \rightarrow R_0^{\pi/2}$ in the toggling frame. The three sections of the sequence are again labelled I, II, and III. The arcs have radius Δ . (b): error integral $\mathbf{p}(t)$ and three error integral vectors \mathbf{p}_i for the spin-echo sequence with detuning error.

sphere, but should not be mistaken as such. Treating $\mathbf{p}(t)$ as the motion of a phantom particle as mentioned previously, we can deduce that since its velocity $\Omega'_1(t)$ rotates at a constant rate, the phantom particle's trajectory is composed of circular arcs, as shown in figure 4.

Step II is a semi-circle while steps I and III are quarter-circles. The three-step walk in the presence of detuning also is not closed, so the spin-echo sequence is not fully-compensating with respect to either amplitude errors or detuning errors.

For the case of amplitude error, the first-order constraint is obeyed provided the initial orientation of the Bloch vector is directed along the z -axis because in that case the cross-product of Eq.(19) is zero. This result can be understood as follows. Suppose that initially the Bloch vector points along the z -axis. The strength of the AC control pulse is somewhat too large, so the Bloch vector slightly overshoots the $-y$ direction during the first $\pi/2$ pulse around the x -axis. To first-order, a small error is generated in the $-z$ direction. The π -pulse along the y -axis flips this error around, causing the Bloch vector to slightly undershoot the $-y$ direction. The π -pulse acts here as a form of “time-reversal”, allowing the third pulse to undo the error caused by the first pulse. This time-reversal is evident in figure 3, as \mathbf{p}_I is anti-parallel with

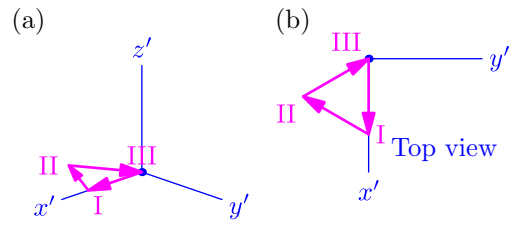


FIG. 5. (a): the three error integral vectors for a three-step π sequence that is fully-compensating to first-order for either kind of error must form an equilateral triangle. The labels I, II, and III refer to the three steps of the sequence. The triangle can be rotated and the direction of the arrows can be inverted. (b): top view.

\mathbf{p}_{II} . A similar argument appealing to spatial reasoning may be made for the case of the detuning error. For detuning error, the first-order constraint is again obeyed if the initial spin orientation is along the x -axis.

B. Three-step Sequences.

For our second example, we will construct three-step sequences that, unlike the spin-echo sequence, are fully-compensating. We restrict ourselves here to sequences of π -pulses in which case the geometrical constructions (N -step walk) can be performed in the horizontal plane. We will “reverse engineer” the sequence, i.e., we construct closed error trajectories in the toggling frame first – which turns out to be straightforward – and then work backwards to find the corresponding sequence in the toggling and lab frames.

With each of the three steps of the sequence, an error integral vector \mathbf{p}_i – with $i = I, II, III$ – is associated. The error integral vectors are now restricted to the xy -plane because the errors represent rotations by π , and they have the same magnitude because the three pulses have the same duration. To produce the closed N -step walk of a fully-compensating sequence there is only one option: the three vectors must form an equilateral triangle (see figure 5). The next steps are finding the corresponding error vectors $\Omega'_1(t)$ – still in the toggling frame – and then reconstructing the corresponding sequence in the lab frame.

The simplest case is again that of an amplitude error because the error $\Omega'_1(t)$ is piece-wise constant and parallel to the pulse direction $\Omega'(t)$ in the toggling frame. Figure 6 shows the three vectorial values that the error $\Omega'_1(t)$ must take during the three steps, which point from the center symmetrically to the vertices of an equilateral triangle. By virtue of the error $\Omega'_1(t)$ being parallel to $\Omega'(t)$, we can immediately read off the pulse directions $\Omega'(t)$ in the toggling frame. It must form the following angles with the x' -axis during the three steps respectively: $0 \rightarrow -2\pi/3 \rightarrow 2\pi/3$. For the case of detuning error, special care needs to be taken in deducing the relationship between the pulse directions $\Omega'(t)$ and \mathbf{p}_i . This is discussed in detail in appendix C, the key conclusion of which is: for detuning error, the direction of \mathbf{p}_i for an odd numbered step is a 90° counter-clockwise rotation from its pulse direction; for

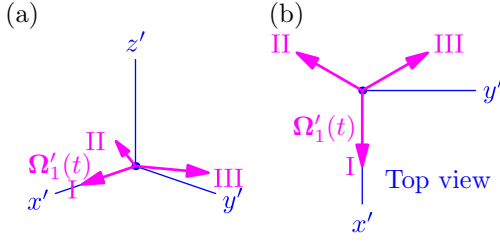


FIG. 6. (a): the three vectorial values taken by the amplitude error $\Omega'_1(t)$ for the three-step π -pulse sequence. The labels I, II, and III refer to the three steps of the sequence. Since $\Omega'_1(t) = \epsilon\Omega'(t)$, we can immediately read off the pulse directions in the toggling frame, which form the following angles with x' -axis: $0 \rightarrow -2\pi/3 \rightarrow 2\pi/3$. (b): top view.

an even numbered step, clockwise.

We are now ready for the final step: the reconstruction of the sequence in the lab frame. Denote this unknown sequence by

$$R_{\phi_1}^\pi \rightarrow R_{\phi_2}^\pi \rightarrow R_{\phi_3}^\pi. \quad (21)$$

For each π -pulse, the lab frame z -axis “toggles” between pointing along z' and $-z'$ direction in the toggling frame. Therefore, the pulse directions, which lie in the xy -plane in the lab frame, lie in the $x'y'$ -plane in the toggling frame. A formula by [Wimperis 1993, Eq 13] relates rotation angles in the lab and toggling frames,

$$\phi'_j = -(-1)^j \phi_j - \sum_{k=1}^{j-1} (-1)^k 2\phi_k, \quad (22)$$

where the $\phi_k = \phi_1, \phi_2, \phi_3, \dots$ specify the pulse directions in the lab frame, and where the ϕ'_j are the corresponding directions in the toggling frame. This transformation is also its own inverse, which means that one can work in the toggling frame and convert the angles back to the lab frame if needed. We first apply this transformation to the case of amplitude error. In the toggling frame, following our previous discussion, the angles between the pulse directions and the x' -axis are $0 \rightarrow -2\pi/3 \rightarrow 2\pi/3$ (figure 6). Converting back to the lab frame angles using Eq.(22), produces the sequence:

$$R_0^\pi \rightarrow R_{2\pi/3}^\pi \rightarrow R_0^\pi. \quad (23)$$

A constant angle can of course be added to all three angles.

Next, for the case of detuning error, we have shown previously that the pulse direction $\Omega'(t)$ needs to form the following three angles with the x' -axis: $0 \rightarrow -\pi/3 \rightarrow -2\pi/3$ (figure 8). Using the transformation formula Eq.(22) produces the composite pulse:

$$R_0^\pi \rightarrow R_{\pi/3}^\pi \rightarrow R_0^\pi. \quad (24)$$

C. Quantum versus Classical Approach

We now are in a position to compare the first-order constraint imposed on the sequences with that of the quantum-

mechanical approach. In Ref.[7, 8] it is shown for the quantum case that for a sequence of π -pulses, the first-order constraints on the orientation angles of the pulse fields impose the conditions

$$\sum_j \sigma_{\phi'_j} = 0 \text{ (amplitude)}, \quad (25)$$

$$\sum_j \sigma_{\phi''_j} = 0 \text{ (detuning)}, \quad (26)$$

where

$$\phi'_j = (-1)^{j+1} \phi_j + \sum_{k < j} (-1)^{k+1} 2\phi_k, \quad (27)$$

$$\phi''_j = \phi'_j + (-1)^{j+1} \pi/2, \quad (28)$$

and where the $\sigma_\phi = \cos \phi \sigma_x + \sin \phi \sigma_y$ are combinations of Pauli matrices. Note that this last relation suggests a link with vectors in the xy -plane.

In order to establish a concrete connection between the quantum and the classical methods, we first formulate the approach described in the previous section in a more mathematical language. We will no longer restrict ourselves to three-step sequences—the sequence will have any odd number of π -pulses—but the key relationships which we illustrated with three-step sequences will remain the same. The following will make precise the relationship between the pulse direction $\Omega(t)$ in the lab frame, the pulse direction $\Omega'(t)$ in the toggling frame, the N -step walk for amplitude error, the N -step walk for detuning error, and the conditions for error-suppression in case of either type of error.

1. Use Eq.(22) to transform from the lab frame pulse directions (ϕ_k) to the toggling frame pulse directions (ϕ'_k).
2. Draw the toggling frame pulse directions as unit length vectors laying in the $x'y'$ -plane. The complex number notation can make this statement more precise: draw the following set of complex numbers as vectors on the complex plane, $\{e^{i\phi'_1}, e^{i\phi'_2}, e^{i\phi'_3} \dots\}$. Label the step number for each vector.
3. (a) To obtain the N -step walk made up of amplitude error integral vectors \mathbf{p}_i : starting from the origin, parallel transport the vectors so that they connect tip-to-tail in order. The final result is the N -step walk made from amplitude error integral vectors \mathbf{p}_i . In terms of complex numbers this can be expressed as:

$$e^{i\phi'_1} + e^{i\phi'_2} + e^{i\phi'_3} + \dots \quad (29)$$

- (b) To obtain the N -step walk made up of detuning error integral vectors \mathbf{p}_i : return to step 2. Rotate those vectors for odd steps counterclockwise by $\pi/2$ and rotate those for the even steps clockwise by $\pi/2$. Starting from the origin, parallel transport the resulting vectors so that they connect tip-to-tail in order. The final result is the N -step walk

made from detuning error integral vectors \mathbf{p}_i . In terms of complex numbers this can be expressed as:

$$ie^{i\phi'_1} - ie^{i\phi'_2} + ie^{i\phi'_3} - \dots \quad (30)$$

Mark the odd steps with “+” signs and even steps with “-” signs on paper.

4. The sequence is fully-compensating to first-order with respect to amplitude error if the figure formed in Eq.(29) is a closed polygon, and it is fully-compensating to first-order with respect to detuning error if the figure formed in Eq.(30) is a closed polygon. In terms of the complex numbers

$$\sum_j e^{i\phi'_j} = 0 \quad (\text{amplitude}), \quad (31)$$

$$\sum_j (-1)^{j-1} ie^{i\phi'_j} = 0 \quad (\text{detuning}). \quad (32)$$

One can check the above algorithm with the three-step sequences in the previous section. The procedure is invertible: one can reverse-engineer a desirable N -step walk to get the specification of the composite pulse, as shown in the discussion of the three-step sequence previously.

Now we can expand our constraints written in complex exponential form in Eq.(31) and (32) into real and imaginary parts, perform the substitution $1 \rightarrow \sigma_x$, $i \rightarrow \sigma_y$, and then use the definition of ϕ''_j from Eq.(28) where appropriate. We obtain

$$\begin{aligned} 0 &= \sum_j e^{i\phi'_j} = \sum_j \cos \phi'_j + i \sin \phi'_j \\ &\Rightarrow (\text{substitution}) \\ 0 &= \sum_j \cos \phi'_j \sigma_x + \sin \phi'_j \sigma_y \\ &= \sum_j \sigma_{\phi'_j} \quad (\text{amplitude error}), \end{aligned}$$

and,

$$\begin{aligned} 0 &= \sum_j (-1)^{j-1} ie^{i\phi'_j} = \sum_j e^{i(\phi'_j + (-1)^{j-1}\pi/2)} \\ &= \sum_j e^{i\phi''_j} = \sum_j \cos \phi''_j + i \sin \phi''_j \\ &\Rightarrow (\text{substitution}) \\ 0 &= \sum_j \cos \phi''_j \sigma_x + \sin \phi''_j \sigma_y \\ 0 &= \sum_j \sigma_{\phi''_j} \quad (\text{detuning error}). \end{aligned}$$

This reproduces Eqs.(25) and (26). In terms of the first-order constraint, the classical and quantum error suppression sequences are the same. See appendix E for a demonstration on how the constraints formulated in this section can be applied on the design of five-step sequences that are fully-compensating to the first order in both amplitude and detuning error.

IV. THE SECOND-ORDER CONSTRAINT.

Second-order errors are eliminated when the constraint Eq.(15) is satisfied. Assume that the first-order constraint is obeyed and substitute the definition of the error integral $\mathbf{p}(t)$ (see Eq.(16)) into the second constraint:

$$\mathbf{r}'_2|_{t=t_f} = \int_0^{t_f} \frac{d}{ds} \mathbf{p}(s) \times (\mathbf{p}(s) \times \mathbf{r}_0(0)) ds. \quad (33)$$

Using the fact that the $\mathbf{p}(t)$ curve is closed, this equation can be manipulated (see appendix D) into the form:

$$\mathbf{r}'_2|_{t=t_f} = \mathbf{r}_0(0) \times \left(\frac{1}{2} \oint \mathbf{p} \times d\mathbf{p} \right). \quad (34)$$

The vector area $\mathbf{A} = \int_S d\mathbf{S}$ of any surface bounded by the same curve \mathcal{C} is given by

$$\mathbf{A} = \frac{1}{2} \oint_C \mathbf{r} \times d\mathbf{r}, \quad (35)$$

where \mathbf{r} traces out the boundary curve [11]. It follows that if the vector area of any surface enclosed by the error integral is zero, then the second-order error is zero independent of the initial condition. The corresponding pulse is then fully-compensating to second-order. Otherwise, the sequence suppresses second-order error only for states initially polarized in the same direction as the vector area.

A. Three-step Sequences.

As a first illustration, the second constraint is applied to the two three-step sequences Eq.(23) and Eq.(24), which were shown to be fully-compensating to first-order for, respectively, amplitude and detuning error. Start with Eq.(23). The signed area enclosed by the vectors I, II, III is an equilateral triangle with normal along the z' direction. The error suppression of this sequence is thus not fully-compensating to second-order though the second-order error does vanish for initial states polarized along the z -axis.

Next, consider the sequence Eq.(24) for the case of detuning error. The enclosed area can be divided into three planar parts bounded by semi-circles plus a planar part bounded by the triangle, as shown in figure 7. The directions of vector areas of the three semi-circles are all in the $x'y'$ plane and thus cannot cancel the vector area of the triangle, which is along the z' direction. It follows that the net vector area is non-zero as well, so this sequence is also *not* fully-compensating to second-order with respect to detuning error. An example of sequences which are fully-compensating to the second order can be found in appendix E which discusses the performance of five-step sequences.

B. Quantum versus Classical Approach.

This suggests that, like the first-order constraint, the classical and quantum conditions for second-order error suppres-

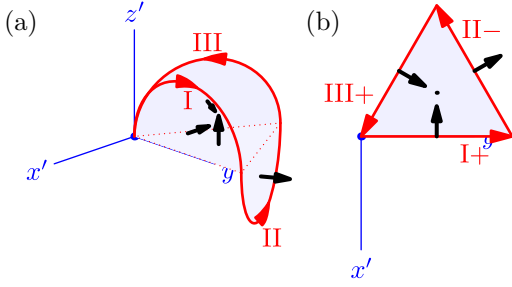


FIG. 7. (a): decomposition of the vector area $\frac{1}{2} \oint \mathbf{p} \times d\mathbf{p}$ enclosed by the detuning error integral $\mathbf{p}(t)$ for the three-step sequence of Eq.(24). The vector areas of each of the four sub-areas are indicated by small black arrows. (b): the three vector areas associated with semi-circle trajectories. A plus sign indicates the semi-circle is above the $z = 0$ plane and a minus sign below the $z = 0$ plane. The vector sum from the semi-circles lies in the $x'y'$ -plane and cannot cancel the vector area of the enclosed triangle which lies along the z' -axis.

sion are equivalent. The formal proof can be sketched as follows. Following [7] the condition for second-order amplitude error suppression in the quantum approach is

$$\sum_j \sum_{k < j} [\sigma_{\phi'_j}, \sigma_{\phi'_k}] = 0 \text{ (amplitude)}. \quad (36)$$

As discussed in Ref. [8] (see Eq.(3)) the sum of commutators in this equation, which is constrained to be zero, is in fact the signed area formed by a walk in the plane defined by the different angles. That can also be seen by rewriting this condition as

$$\sum_j \sum_{k < j} \sin(\phi'_j - \phi'_k) \sigma_z = 0, \quad (37)$$

and recalling that the cross-product of two unit vectors is the vector area of the parallelogram spanned by the two unit vectors. Similarly, the condition for the second-order detuning error is

$$\sum_j \sum_{k < j} \sin(\phi''_j - \phi''_k) \sigma_z = 0 \text{ (detuning)}. \quad (38)$$

For the amplitude and detuning errors, the signed area formed by the walk in the plane specified by the different angles must be zero.

V. CONCLUSION.

In conclusion, we have shown that the suppression of systematic amplitude and detuning errors using composite pulses depends minimally on quantum mechanics, and can be described by a combination of the classical mechanics of Larmor precession and simple vector algebra. The focus of this paper has been mostly placed on sequences with an odd number of π -pulses. The technique is less straightforward for the case of constructing error-suppressing sequences from $\pi/2$ -pulses because the closed walk of \mathbf{p}_i vectors would no longer be

planar. Sequences of $\pi/2$ pulses is nevertheless a promising direction, because the extra spatial degree of freedom could allow for shorter sequences given the same order of error suppression. A related, but distinct, direction for potential development is to apply it to sequences that accomplish a net $\pi/2$ -pulse (or any other fractional- π pulses) rather than just a π -pulse. Such strategies have been proposed in the literature: one could prepend or append any number of correcting π or 2π -pulses to the target pulse. The bulk of the spin evolution in this case would still produce $\mathbf{p}(t)$ curves which are planar so the technique developed in this paper would still be applicable.

Because of our classical treatment of the evolution of the spin, information about the global phase of the qubit is lost entirely. This, incidentally, raises the question whether it is possible to achieve even better amplitude and detuning error suppression utilizing truly quantum mechanical properties of the qubit. The classical framework is in general not applicable if one is concerned with questions involving the phase of the qubit. For example, if there is an error in the overall phase of the composite pulse, then suppressing that would be beyond the range of the classical approach. The classical framework also can not accommodate problems involving the performance of a sequence when interactions with the environment lead to phase-decoherence. Another important assumption was that the amplitude or detuning errors are constant in time. In actuality, often a drift occurs over time. To model the drift in the experimental parameters one could allow for different errors for each step in the sequence, i.e. a set of $\{\epsilon_1, \epsilon_2, \epsilon_3, \dots\}$ or $\{\delta_1, \delta_2, \delta_3, \dots\}$. The steps of the error integral vectors would no longer be of equal length in that case. The solution of the constraints would follow the same geometric principles, but it would be more mathematically involved.

Acknowledgements: I would like to thank R. Bruinsma, W. Campbell and C. Romes for guidance, insights, and discussions and R. Bruinsma for assistance in the preparation of the manuscript. Initial work on this project was carried out by Xingchen Fan and Clementine Domine with support from the NSF-DMR under CMMT Grant 1836404.

Appendix A: Rotating Wave Approximation and the Classical Equation of Motion.

Begin with the *lab-frame* Hamiltonian

$$H = \hbar/2[\omega_0 \hat{\sigma}_z + \Omega \cos(\omega t + \phi) \hat{\sigma}_x + \Omega \sin(\omega t + \phi) \hat{\sigma}_y], \quad (A1)$$

which describes the rotation of the spin under the DC and AC magnetic field. Following [9], cancel the spin precession caused by the DC field with the rotating wave approximation. Define

$$|\psi\rangle = U(t) |\psi\rangle^{rot}, \quad (A2)$$

where $U = \exp(-\frac{i\omega t}{2} \hat{\sigma}_z)$ is a rotation about the z -axis. Plugging in this definition into the Schrodinger's equation $i\partial_t |\psi\rangle = H |\psi\rangle$ produces the effective Hamiltonian

$$H' = U^\dagger H U - i\hbar U^\dagger \frac{dU}{dt}. \quad (A3)$$

Notice that

$$\cos \theta \hat{\sigma}_x + \sin \theta \hat{\sigma}_y = e^{-i\theta \hat{\sigma}_z} \hat{\sigma}_x = \hat{\sigma}_x e^{i\theta \hat{\sigma}_z}. \quad (\text{A4})$$

Hence

$$\begin{aligned} & U^\dagger (\cos(\omega t + \phi) \hat{\sigma}_x + \sin(\omega t + \phi) \hat{\sigma}_y) U \\ &= e^{\frac{i\omega t}{2} \hat{\sigma}_z} \left(e^{-i(\omega t + \phi) \hat{\sigma}_z} \hat{\sigma}_x \right) e^{-\frac{i\omega t}{2} \hat{\sigma}_z} \\ &= e^{\frac{i\omega t}{2} \hat{\sigma}_z} e^{-i(\omega t + \phi) \hat{\sigma}_z} e^{\frac{i\omega t}{2} \hat{\sigma}_z} \hat{\sigma}_x \\ &= e^{-i\phi \hat{\sigma}_z} \hat{\sigma}_x \\ &= \cos \phi \hat{\sigma}_x + \sin \phi \hat{\sigma}_y. \end{aligned} \quad (\text{A5})$$

Because U commutes with $\hat{\sigma}_z$ and $U^\dagger \frac{dU}{dt} = -i\omega \hat{\sigma}_z / 2$, the effective Hamiltonian is

$$H' = \hbar/2 [(\omega_0 - \omega) \hat{\sigma}_z + \Omega \cos \phi \hat{\sigma}_x + \Omega \sin \phi \hat{\sigma}_y]. \quad (\text{A6})$$

In the case where the AC magnetic field is linearly polarized as opposed to circularly polarized, the field can be decomposed into two counter-rotating circularly polarized waves. The lab-frame Hamiltonian will have the term

$$H_{\text{rf}} = 2\Omega \cos(\omega t + \phi) \hat{\sigma}_x \quad (\text{A7})$$

$$\begin{aligned} &= \Omega (\cos(\omega t + \phi) \hat{\sigma}_x + \sin(\omega t + \phi) \hat{\sigma}_y) \\ &\quad + \Omega (\cos(\omega t + \phi) \hat{\sigma}_x - \sin(\omega t + \phi) \hat{\sigma}_y). \end{aligned} \quad (\text{A8})$$

Under the unitary transformation $U^\dagger H_{\text{rf}} U$, the second term above produces

$$\begin{aligned} & U^\dagger (\cos(\omega t + \phi) \hat{\sigma}_x - \sin(\omega t + \phi) \hat{\sigma}_y) U \\ &= e^{\frac{i\omega t}{2} \hat{\sigma}_z} \left(e^{i(\omega t + \phi) \hat{\sigma}_z} \hat{\sigma}_x \right) e^{-\frac{i\omega t}{2} \hat{\sigma}_z} \\ &= e^{\frac{i\omega t}{2} \hat{\sigma}_z} e^{i(\omega t + \phi) \hat{\sigma}_z} e^{\frac{i\omega t}{2} \hat{\sigma}_z} \hat{\sigma}_x \\ &= e^{i(2\omega t + \phi) \hat{\sigma}_z} \hat{\sigma}_x. \end{aligned}$$

If the drive frequency ω is close to the Larmor frequency ω_0 , then this high frequency time-dependent term has only a minor effect and is dropped in the rotating wave approximation. Hence the wave rotating against the Larmor precession caused by the DC field can be neglected.

Now define the vector $\boldsymbol{\Omega} = (\Delta, \Omega \cos \phi, \Omega \sin \phi)$, where, $\Delta = \omega_0 - \omega$. Then the effective Hamiltonian in the rotating frame is

$$H' = \frac{\hbar}{2} \boldsymbol{\Omega} \cdot \boldsymbol{\sigma}. \quad (\text{A9})$$

By Ehrenfest Theorem, the evolution of the Bloch vector is

$$\frac{d\langle \hat{\sigma}_k \rangle}{dt} = \left\langle \frac{i}{\hbar} [H', \hat{\sigma}_k] \right\rangle + \left\langle \frac{\partial \hat{\sigma}_k}{\partial t} \right\rangle. \quad (\text{A10})$$

The time derivative of the operator vanishes. The commutator can be evaluated

$$[H', \hat{\sigma}_k] = \frac{\hbar}{2} \Omega_j [\hat{\sigma}_j, \hat{\sigma}_k] = \frac{\hbar}{2} \Omega_j (2i\epsilon_{jkl} \hat{\sigma}_l) = -i\hbar \epsilon_{jlk} \Omega_j \hat{\sigma}_l. \quad (\text{A11})$$

Therefore,

$$\begin{aligned} \frac{d\langle \hat{\sigma}_k \rangle}{dt} &= \epsilon_{jlk} \Omega_j \langle \hat{\sigma}_l \rangle \\ \frac{d\langle \boldsymbol{\sigma} \rangle}{dt} &= \boldsymbol{\Omega} \times \langle \boldsymbol{\sigma} \rangle. \end{aligned} \quad (\text{A12})$$

Appendix B: Transformation into the Toggling Frame.

This section is concerned with solving the equation

$$\frac{d\mathbf{r}(t)}{dt} = (\boldsymbol{\Omega}(t) + \boldsymbol{\Omega}_1(t)) \times \mathbf{r}(t), \quad (\text{B1})$$

by introducing the toggling frame controlled by the rotation operator $\hat{\mathbf{R}}$, which is the solution to the operator equation

$$\frac{d}{dt} \hat{\mathbf{R}}(t) = \boldsymbol{\Omega}(t) \times \hat{\mathbf{R}}(t), \quad (\text{B2})$$

with initial condition $\hat{\mathbf{R}}(0) = \hat{\mathbf{1}}$. Let the motion of the Bloch vector be the composition of both the rotation of the toggling frame and the motion with respect to the toggling frame, i.e. $\mathbf{r}(t) = \hat{\mathbf{R}}(t) \mathbf{r}'(t)$, where $\mathbf{r}'(t)$ is the Bloch vector in the toggling frame. Direct substitution into Eq. (B1) gives

$$\frac{d}{dt} (\hat{\mathbf{R}} \mathbf{r}') = (\boldsymbol{\Omega} + \boldsymbol{\Omega}_1) \times (\hat{\mathbf{R}} \mathbf{r}') \quad (\text{B3})$$

$$\left(\frac{d}{dt} \hat{\mathbf{R}} \right) \mathbf{r}' + \hat{\mathbf{R}} \frac{d\mathbf{r}'}{dt} = (\boldsymbol{\Omega} + \boldsymbol{\Omega}_1) \times (\hat{\mathbf{R}} \mathbf{r}'), \quad (\text{B4})$$

where the time-dependence is suppressed in the notation. Using Eq.(B2), for the time derivative of $\hat{\mathbf{R}}$,

$$\boldsymbol{\Omega} \times (\hat{\mathbf{R}} \mathbf{r}') + \hat{\mathbf{R}} \frac{d\mathbf{r}'}{dt} = (\boldsymbol{\Omega} + \boldsymbol{\Omega}_1) \times (\hat{\mathbf{R}} \mathbf{r}'). \quad (\text{B5})$$

The two terms involving $\boldsymbol{\Omega}$ can be cancelled,

$$\hat{\mathbf{R}} \frac{d\mathbf{r}'}{dt} = \boldsymbol{\Omega}_1 \times (\hat{\mathbf{R}} \mathbf{r}'). \quad (\text{B6})$$

Multiplication by the inverse of the operator $\hat{\mathbf{R}}$ on both sides,

$$\frac{d\mathbf{r}'}{dt} = \hat{\mathbf{R}}^{-1} (\boldsymbol{\Omega}_1 \times (\hat{\mathbf{R}} \mathbf{r}')). \quad (\text{B7})$$

If $\boldsymbol{\Omega}_1(t) = 0$, then the time derivative of $\mathbf{r}'(t)$ must vanish, and the Bloch vector merely rotates with the toggling frame, as should be expected in the absence of errors. If errors are present and $\boldsymbol{\Omega}_1(t) \neq 0$, one can use the following identity to distribute the inverse rotation operator $\hat{\mathbf{R}}^{-1}$ into both operands of the cross product:

$$(\hat{\mathbf{R}} \mathbf{A}) \times (\hat{\mathbf{R}} \mathbf{B}) = \hat{\mathbf{R}} (\mathbf{A} \times \mathbf{B}), \quad (\text{B8})$$

where $\hat{\mathbf{R}}$ is a proper rotation and \mathbf{A}, \mathbf{B} are any pair of 3D vectors. Therefore

$$\frac{d\mathbf{r}'}{dt} = \hat{\mathbf{R}}^{-1} (\boldsymbol{\Omega}_1 \times (\hat{\mathbf{R}} \mathbf{r}')) \quad (\text{B9})$$

$$= (\hat{\mathbf{R}}^{-1} \boldsymbol{\Omega}_1) \times (\hat{\mathbf{R}}^{-1} \hat{\mathbf{R}} \mathbf{r}') \quad (\text{B10})$$

$$= (\hat{\mathbf{R}}^{-1} \boldsymbol{\Omega}_1) \times \mathbf{r}'. \quad (\text{B11})$$

Now one can define the vector $\boldsymbol{\Omega}'_1(t) = \hat{\mathbf{R}}(t)^{-1} \boldsymbol{\Omega}_1(t)$. The application of $\hat{\mathbf{R}}^{-1}(t)$ on the un-primed vectors, such as in

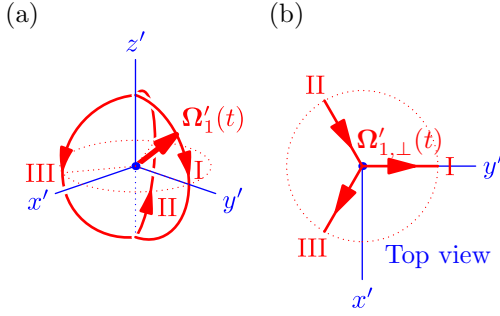


FIG. 8. (a): time-dependence of detuning error $\Omega'_1(t)$ for the three-step π -pulse sequence, by symmetry argument. The labels I, II, and III refer to the three steps of the sequence. Note in particular the direction of traversal labelled on each arc, especially for step II. At $t = 0$, Ω'_1 must point in the z' direction because at this point the toggle frame axes coincide with the lab frame axes. (b): top view.

the case of $\mathbf{r}(t)$, produces the coordinates of the vector in the toggling frame. Therefore $\Omega'_1(t)$ is the error vector viewed in the toggling frame. Finally, one obtains the equation of motion for the Bloch vector in the toggling frame,

$$\frac{d\mathbf{r}'(t)}{dt} = \Omega'_1(t) \times \mathbf{r}'(t), \quad (\text{B12})$$

with the time dependence restored in notation.

Appendix C: Relationship between $\Omega'_1(t)$ and \mathbf{p}_i for Detuning Error.

Since we are only considering composite pulses consisting of three π -pulses, the trajectory of the error $\Omega'_1(t)$ for the detuning case must consist of three semi-circular arcs. By symmetry, for the integral in Eq.(16) to vanish and the walk to close, one may postulate that the planes of the three arcs must make angles of $2\pi/3$, so that the figure formed has its center of mass located at the origin, as shown in figure 8.

It is necessary to draw this previous reasoning for the detuning case back to the equilateral triangle we began with. Treating the $\Omega'_1(t)$ as the time-dependent velocity of a phantom particle performing uniform circular motion, it follows from figure 9 that the three error integral vectors so generated indeed form an equilateral triangle, and $\Omega'_1(t)$ is the unique way this can happen. Notice in particular that the angle formed between the planes of the semi-circles in figure 8 coincides with the angles formed between \mathbf{p}_i and the x' -axis in figure 9.

Some additional work needs to be done in order to read off the pulse direction required in the toggling frame from figure 8. Recall that in case of detuning error, the apparent motion of $\Omega'_1(t)$ in the toggling frame, such as that in figure 8 is caused by the rotation of the toggling frame itself, while the vector $\Omega_1 = \Delta\hat{z}$ in truth stays constant in the lab frame. To generate the apparent rotation of $\Omega'_1(t)$ as seen in step I in the toggling frame, the pulse direction must be in the x' direction—rather than in the $-x'$ direction, as one might expect if one naively uses the right-hand-rule on arc I. Similar arguments can be

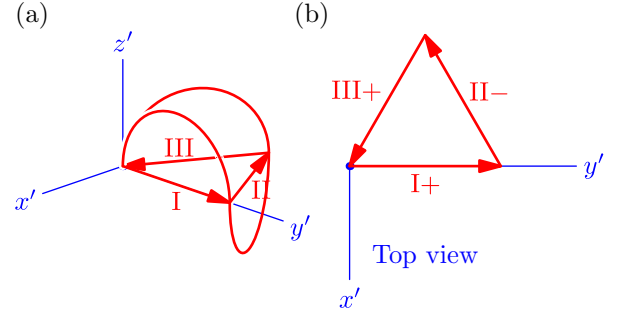


FIG. 9. The detuning error integral vectors \mathbf{p}_i in the three-step sequence $R_0^\pi \rightarrow R_{\pi/3}^\pi \rightarrow R_0^\pi$. (a): each π -pulse produces a semicircular trajectory whose net effect is a translation along straight lines in the $x'y'$ -plane, forming the three error integral vectors. (b): the same curve viewed from the top. A plus or a minus sign is marked depending on whether the curve threads above or under the $z = 0$ plane.

carried out for step II and III. As a result, the pulse directions must form the following angles with the x' -axis during the three steps respectively: $0 \rightarrow -\pi/3 \rightarrow -2\pi/3$.

Now compare these angles with those formed between \mathbf{p}_i and the x' -axis in figure 9. If one take the angles from the pulse direction of odd numbered steps in the toggling frame and add $\pi/2$, one obtains the angle for \mathbf{p}_i . For even numbered steps (step II only, in this case) addition by $\pi/2$ is replaced by subtraction by $\pi/2$. This relationship will help us generalize to longer sequences. The differentiated treatment between even and odd numbered steps can be explained by the fact that the direction of traversal of the semi-circles in figure 8 toggles between top-to-bottom and bottom-to-top.

Appendix D: Manipulating the Second-order Constraint.

Substitute the definition of $\mathbf{p}(t)$ into the second-order constraint to obtain

$$\begin{aligned} \mathbf{r}'_2|_{t=0}^{t_f} &= \int_0^{t_f} \dot{\mathbf{p}}(s) \times (\mathbf{p}(s) \times \hat{\mathbf{u}}) ds \\ &= \int [(\dot{\mathbf{p}} \cdot \hat{\mathbf{u}})\mathbf{p} - (\dot{\mathbf{p}} \cdot \mathbf{p})\hat{\mathbf{u}}] ds, \end{aligned} \quad (\text{D1})$$

where the simplified notation $\hat{\mathbf{u}} = \mathbf{r}_0(0)$ is used for the initial condition. The second term is easily integrated since $\dot{\mathbf{p}} \cdot \mathbf{p} = \frac{1}{2} \frac{d}{dt} \mathbf{p}^2$. The first term contains such terms as $p_x dp_z$, and $p_y dp_z$, which motivates one to consider the area integral $\frac{1}{2} \int \mathbf{p} \times \dot{\mathbf{p}} ds$. Using vector identities and the fact that the $\mathbf{p}(t)$ curve is closed, Eq.(D1) can be manipulated by following the logic below,

$$\begin{aligned} \hat{\mathbf{u}} \times (\mathbf{p} \times \dot{\mathbf{p}}) &= (\dot{\mathbf{p}} \cdot \hat{\mathbf{u}})\mathbf{p} - (\mathbf{p} \cdot \hat{\mathbf{u}})\dot{\mathbf{p}} \\ &= 2(\dot{\mathbf{p}} \cdot \hat{\mathbf{u}})\mathbf{p} - (\dot{\mathbf{p}} \cdot \hat{\mathbf{u}})\mathbf{p} - (\mathbf{p} \cdot \hat{\mathbf{u}})\dot{\mathbf{p}} \\ &= 2(\dot{\mathbf{p}} \cdot \hat{\mathbf{u}})\mathbf{p} - \frac{d}{dt} [(\mathbf{p} \cdot \hat{\mathbf{u}})\mathbf{p}] \\ (\dot{\mathbf{p}} \cdot \hat{\mathbf{u}})\mathbf{p} &= \hat{\mathbf{u}} \times \frac{1}{2} (\mathbf{p} \times \dot{\mathbf{p}}) + \frac{1}{2} \frac{d}{dt} [(\mathbf{p} \cdot \hat{\mathbf{u}})\mathbf{p}]. \end{aligned} \quad (\text{D2})$$

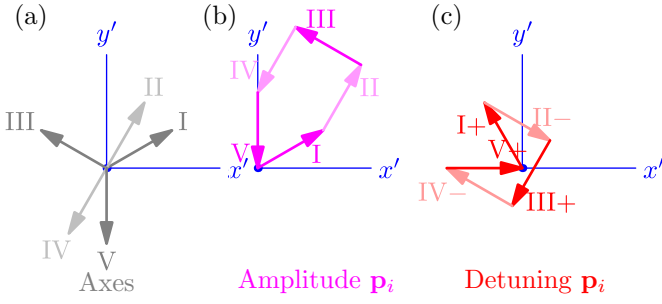


FIG. 10. (a) The five pulse directions, (b) amplitude and (c) detuning error integral vectors \mathbf{p}_i for the Knill sequence in the toggling frame. The \mathbf{p}_i vectors form five-step closed walks in both cases. The even steps are colored lighter.

Hence,

$$\begin{aligned} \mathbf{r}'_2|_{t=t_f} &= \hat{\mathbf{u}} \times \frac{1}{2} \int_0^{t_f} \mathbf{p} \times \dot{\mathbf{p}} ds + \frac{1}{2} [(\mathbf{p} \cdot \hat{\mathbf{u}})\mathbf{p} - \mathbf{p}^2 \hat{\mathbf{u}}]_{s=0}^{t_f} \\ &= \hat{\mathbf{u}} \times \frac{1}{2} \int_0^{t_f} \mathbf{p} \times \dot{\mathbf{p}} ds + \frac{1}{2} [\mathbf{p} \times (\mathbf{p} \times \hat{\mathbf{u}})]_{s=0}^{t_f}. \end{aligned} \quad (\text{D3})$$

If the composite pulse already fully compensates either kind of first-order error, then the $\mathbf{p}(t)$ curve for said error is necessarily closed, and the boundary term in the integral vanishes. One obtains

$$\mathbf{r}'_2|_{t=t_f} = \hat{\mathbf{u}} \times \left(\frac{1}{2} \oint \mathbf{p} \times d\mathbf{p} \right). \quad (\text{D4})$$

Appendix E: Five-step Sequences.

As an illustration of the mapping between the quantum and classical approaches, and as another application of the toggling formula Eq.(22), we consider here the Knill sequence [6], the five-step sequence, mentioned in the Introduction, that provides effective amplitude and detuning error suppression. In our notation, the Knill sequence takes the form,

$$R_{\pi/6}^\pi \rightarrow R_0^\pi \rightarrow R_{\pi/2}^\pi \rightarrow R_0^\pi \rightarrow R_{\pi/6}^\pi. \quad (\text{E1})$$

Using Eq.(22) this translates to toggling frame phases $\pi/6 \rightarrow \pi/3 \rightarrow 5\pi/6 \rightarrow -2\pi/3 \rightarrow -\pi/2$. The corresponding five \mathbf{p}_i vectors for amplitude and detuning errors are shown in figure 10. The five-step walks are closed in both cases. The Knill sequence is thus fully-compensating to first-order with respect to both amplitude and detuning error. Note that the error integral vectors of the odd steps (i.e., steps I, III, and V) still form an equilateral triangle while the even steps (i.e., steps II and IV) are anti-parallel and thus cancel.

The same algorithm can be used to identify other five-step sequences composed of π -pulses that share these same properties. Treat the five pulse-direction angles ϕ'_i as variables. According to the algorithm, the conditions for full compensa-

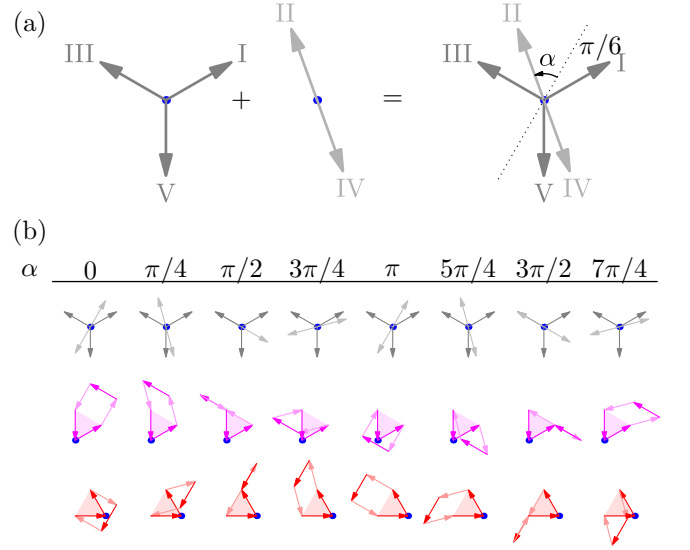


FIG. 11. (a): definition of the undetermined angle α of the Knill sequence family, with $\alpha = 0$ the original Knill sequence. (b, top row): examples of the pulse directions, amplitude and detuning \mathbf{p}_i for different α . Sections of the walks that are invariant under changes of α are highlighted. (b, middle row): amplitude error walk. (b, bottom row): detuning error walk. Note the geometrical similarity of amplitude and detuning walks as α varies.

tion of amplitude and detuning error to first-order are

$$e^{i\phi'_1} + e^{i\phi'_2} + e^{i\phi'_3} + e^{i\phi'_4} + e^{i\phi'_5} = 0, \quad (\text{E2})$$

$$ie^{i\phi'_1} - ie^{i\phi'_2} + ie^{i\phi'_3} - ie^{i\phi'_4} + ie^{i\phi'_5} = 0. \quad (\text{E3})$$

The two conditions are obeyed if

$$e^{i\phi'_1} + e^{i\phi'_3} + e^{i\phi'_5} = 0, \quad (\text{E4})$$

$$e^{i\phi'_2} + e^{i\phi'_4} = 0. \quad (\text{E5})$$

The geometric meaning of these conditions is as follows: the three \mathbf{p}_i vectors for odd i must form an equilateral triangle while the two \mathbf{p}_i vectors for even i must be anti-parallel. Ignoring inversion and global rotation, one is left with an undetermined relative angle α between the odd and even steps. In the toggling frame, the pulse directions are $\pi/6 \rightarrow (\pi/3 + \alpha) \rightarrow 5\pi/6 \rightarrow (-2\pi/3 + \alpha) \rightarrow -\pi/2$, where $\alpha = 0$ corresponds to the original Knill sequence.

The corresponding sequence in the lab frame are

$$R_{\pi/6+2\alpha}^\pi \rightarrow R_\alpha^\pi \rightarrow R_{\pi/2}^\pi \rightarrow R_{-\alpha}^\pi \rightarrow R_{\pi/6-2\alpha}^\pi. \quad (\text{E6})$$

This should be compared with the family of five-step composite pulses that was obtained using the full machinery of quantum mechanics (see Eq.(47) of Ref.[7]). The angles which determine the pulse directions are:

$$\phi = (\pi + 2\alpha', \alpha', -\pi/3, -5\pi/3 - \alpha', -7\pi/3 - 2\alpha') \quad (\text{E7})$$

depending on a single parameter α' . All members of this family are fully-compensating to first-order against amplitude and

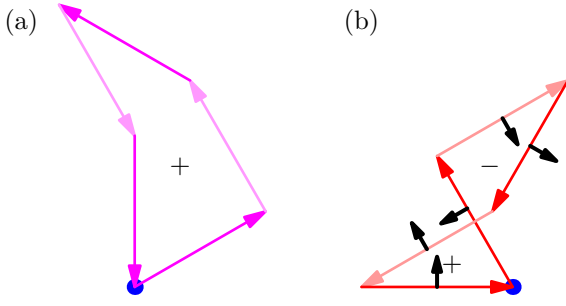


FIG. 12. The vector area enclosed by the five-step walk for $\alpha = \pi/3$. (a): top view of the planar five-step walk for amplitude error. The vector area is non-zero and directed along z' . (b): top view of the non-planar detuning $\mathbf{p}(t)$ curve. This polygon also has non-zero area for most α . The red polygon in this picture has area which is near zero. Black: the positive direction of the area contribution from the five semi-circles in the detuning $\mathbf{p}(t)$ curve. Blue: the origin of the toggling frame.

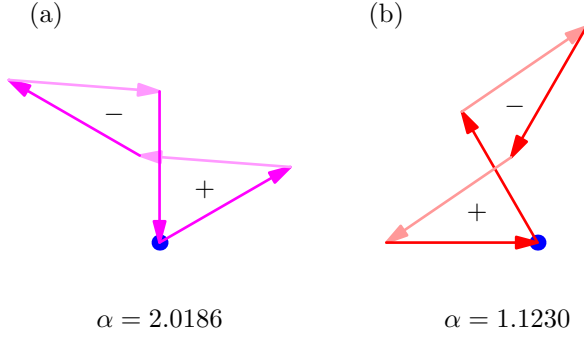


FIG. 13. Polygons associated with second-order fully-compensating five-step sequences. Both polygons have zero net area. (a): The sequence with $\alpha = 2.0186$ is fully-compensating against amplitude error. (b): the sequence with $\alpha = 1.1230$ is fully-compensating against detuning error. The $+/-$ signs indicate the signed contribution to the total vector area of the enclosed figure. Blue dot: the origin of the toggling frame.

detuning errors. When $\alpha' = 7\pi/6$, the Knill sequence results. Although the α parameter of Eq.(E6) is shifted with respect to α' , it is clear that the two expressions describe the same family, except that all angles differ by a constant $7\pi/6$.

As a second illustration, the second-order constraint is applied to the family of five-step sequences that obeys the first-order constraint. The five \mathbf{p}_i vectors of the five-step closed walks for α equal to $\pi/3$ are shown in figure 12 both for amplitude (a) and detuning error (b). For the case of amplitude error, the $\mathbf{p}(t)$ curve is strictly planar so the direction of the vector area is in general along the z' direction. The area of the enclosed pentagonal figure is its magnitude. The second-order constraint for amplitude error is thus not obeyed for $\alpha = \pi/3$.

For the case of the detuning error, the family of five-step Knill-like sequences has the property that the vector area contributed by the five semi-circles in the detuning $\mathbf{p}(t)$ curve exactly cancel (by virtue of the separate cancellation among odd steps and even steps). Only a pentagonal area is left. As shown in figure 12, for $\alpha = \pi/3$ the pentagon is self-intersecting, breaking up the figure in two separate parts. The vector area of the two parts have sign and point in opposite direction. For $\alpha = \pi/3$, the two contributions nearly cancel. This suggests that for general α the five-step sequence is not fully-compensating but there could be a special value of α close to $\alpha = \pi/3$ for which there is an exact cancellation. As shown in figure 13, this is indeed the case for $\alpha = \pm \left(\pi - \arccos \left(-\frac{\sqrt{3}}{4} \right) \right) = \pm 1.1230$. We will denote this as a “magic angle”. The value of the magic angle is calculated by equating the area of the parallelogram formed by steps II, III, and, IV of the five-step sequence to the area of the equilateral triangle formed by steps I and V. Similarly, for $\alpha = \pm \arccos \left(-\frac{\sqrt{3}}{4} \right) = \pm 2.0186$, the amplitude $\mathbf{p}(t)$ curve has zero vector area, and the corresponding sequence is fully-compensating to the second-order with respect to amplitude error.

[1] G. H. Low, T. J. Yoder, and I. L. Chuang, *Phys. Rev. A* **89**, 022341 (2014), publisher: American Physical Society.
 [2] A. M. Steane, *Phys. Rev. Lett.* **77**, 793 (1996).
 [3] P. W. Shor, *Phys. Rev. A* **52**, R2493 (1995).
 [4] D. Manzano, *AIP Advances* **10**, 025106 (2020), <https://doi.org/10.1063/1.5115323>.
 [5] C. A. Ryan, J. S. Hodges, and D. G. Cory, *Phys. Rev. Lett.* **105**, 200402 (2010), publisher: American Physical Society.
 [6] A. M. Souza, G. A. Alvarez, and D. Suter, *Phys. Rev. Lett.* **106**, 240501 (2011).
 [7] J. A. Jones, *Phys. Rev. A* **87**, 052317 (2013), publisher: Amer-

ican Physical Society.
 [8] J. T. Merrill, S. C. Doret, G. Vittorini, J. P. Addison, and K. R. Brown, *Phys. Rev. A* **90**, 040301 (2014), publisher: American Physical Society.
 [9] L. M. K. Vandersypen and I. L. Chuang, *Rev. Mod. Phys.* **76**, 1037 (2005), publisher: American Physical Society.
 [10] M. H. Levitt and R. Freeman, *Journal of Magnetic Resonance* (1969) **33**, 473 (1979).
 [11] D. J. Griffiths, *Introduction to electrodynamics* (Pearson Education, 2014).